Journal of Molecular Graphics and Modelling 58 (2015) 30–39

Contents lists available at ScienceDirect

Journal of Molecular Graphics and Modelling

journal homepage: www.elsevier.com/locate/JMGM

Revised force-field parameters for chlorophyll-*a*, pheophytin-*a* and plastoquinone-9

Federico Guerra, Suliman Adam, Ana-Nicoleta Bondar*

Theoretical Molecular Biophysics, Department of Physics, Freie Universitaet Berlin, Arnimallee 14, D-14195 Berlin, Germany

ARTICLE INFO

Article history:
Accepted 3 March 2015
Available online 10 March 2015

Keywords:
CHARMM potential energy function
CHARMM force field parameters
Chlorophyll-*a*
Plastoquinone-9
Pheophytin-*a*
Photosystem II

ABSTRACT

Biological photosynthetic machineries, such as photosystem I, photosystem II, or the bacterial reaction center, use cofactor molecules that absorb light or directly participate in chemical reactions. Accurate description of the structure of the cofactors, and of their interactions with protein groups, is an important step toward understanding how photosynthetic machineries work. Here we revisit the classical force field parameters for chlorophyll-*a*, pheophytin-*a* and plastoquinone-9. We present systematic quantum mechanical and classical mechanical computations that lead to a good description of the structure and non-bonded interactions of these cofactors.

1. Introduction

Photosystem I and photosystem II, found in plants and cyanobacteria, are large protein/cofactor complexes that use the energy of absorbed photons to catalyze complex chemical reactions. Photosystem I transfers electrons across the thylakoid membrane [13], whereas photosystem II splits two water molecules into protons, electrons, and molecular oxygen (for a review see, e.g., ref. [3]). In photosynthetic bacteria, reaction centers consisting of proteins and bound cofactors catalyze light-induced charge separation [26]. Cofactors associated with photosynthetic machineries include chlorophyll-*a* (Chl-*a*) and pheophytin-*a* (Phe-*a*) (in bacteria, bacteriochlorophyll and bacteriopheophytin), carotenoids, quinones, heme groups, non-haem iron and metal clusters (see, for example, Refs. [3,13,26]). Though the molecular motions along the reaction cycles of the photosynthetic machineries are poorly understood, dynamics and interactions with the environment appear important. For example, hydration and protein flexibility appear important for the water cleavage functionality of photosystem II [18], and structural rearrangements of the Mn_4CaO_5 metal cluster and of protein groups may occur during the reaction cycle [19].

Molecular dynamics simulation techniques allow us to probe the dynamics of biomolecular complexes in fluid, solvated environments. A key ingredient of the simulations is the set of force field parameters used to describe bonded and non-bonded interactions among the atoms of the system. Here we present improved CHARMM (Chemistry at HARvard Macromolecular Mechanics, [5]) force field parameters for the electrostatic interactions and geometries of Chl-*a*, Phe-*a* and plastoquinone-9 (Pl-9). Chl-*a* ($C_{55}H_{72}MgN_4O_5$, Fig. 1A and B) is particularly abundant in photosystems I and II: structures of photosystem I from *Synechococcus elongatus* (reviewed in Ref. [13]) and of photosystem II from Thermosynechococcus elongatus [20] *and Thermosynechococcus vulcanus* [30,31] indicate coordinates for 96 and, respectively, 35 Chl-*a* molecules. In photosystem II, the Chl-*a* molecules are located within the transmembrane region of the complex (Fig. 1A), and participate in energy transfer and electron transfer reactions [7,20]. Phe-*a* is similar to Chl-*a*, but the magnesium ion is replaced by two hydrogen atoms covalently bound to nitrogen atoms of the chlorin ring ($C_{55}H_{74}N_4O_5$, Fig. 1C); in photosystem II, Phe-*a* is involved in electron transfer [1,17]. Pl-9 ($C_{53}H_{80}O_2$, Fig. 1D), found in two copies per photosystem II monomer, is involved in electron and proton transfer reactions [28].

The CHARMM potential energy function [5,6,23] consists of a sum of contributions from bonded and nonbonded interactions:

$$E_{MM} = \sum_{bonds} k_b(b-b_0)^2 + \sum_{angles} k_\theta(\theta-\theta_0)^2 + \sum_{dihedrals} k_\phi(1+\cos(n\phi-\delta)) + \sum_{impropers} k_\omega(\omega-\omega_0)^2 + \sum_{Urey-Bradley} (r_{1-3}-r_{1-3,0})^2 + E_{CMAP} + \sum_{Coulomb} \frac{q_i q_j}{\varepsilon r_{ij}} + \sum_{vanderWaals} \varepsilon_{ij}\left[\left(\frac{R_{ij,\min}}{r_{ij}}\right)^{12} - 2\left(\frac{R_{ij,\min}}{r_{ij}}\right)^{6}\right] \quad (1)$$

* Corresponding author. Tel.: +49 30 838 53583.
E-mail address: nbondar@zedat.fu-berlin.de (A.-N. Bondar).

http://dx.doi.org/10.1016/j.jmgm.2015.03.001
1093-3263/

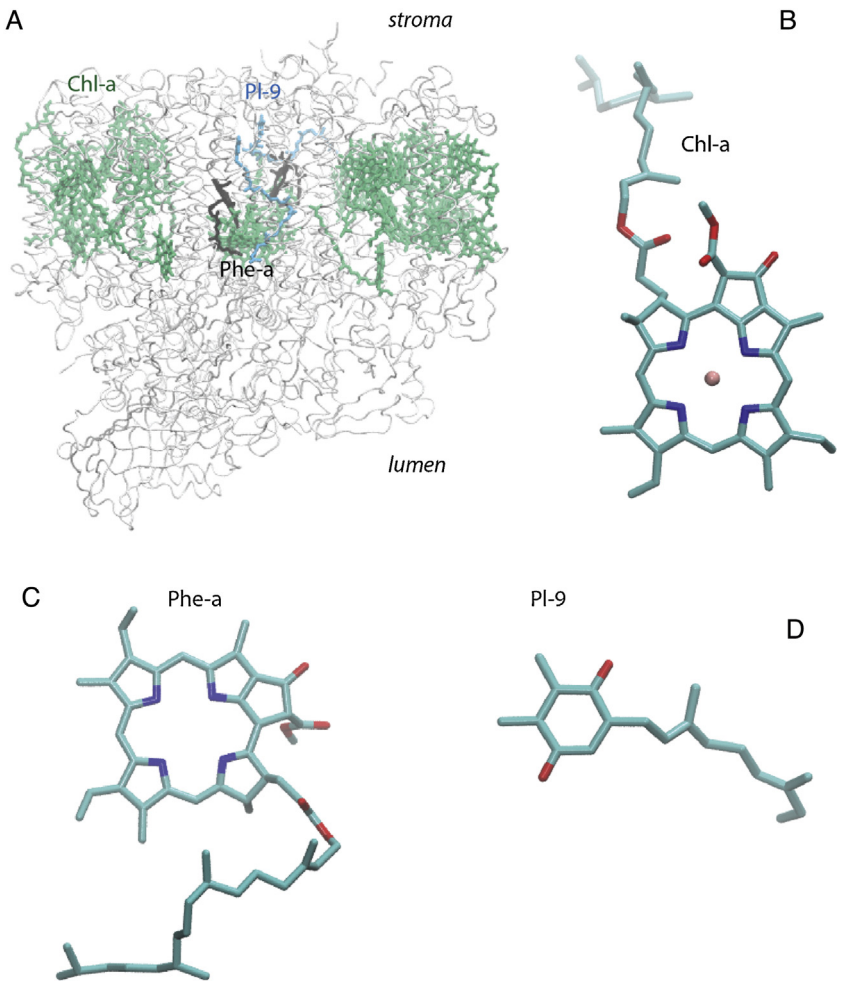

Fig. 1. The Chl-*a*, Phe-*a* and Pl-9 cofactors in photosystem II. (A) Molecular graphics of monomer A of photosystem II from the crystal structure of Ref. [31] (PDB ID: 3ARC). The protein is shown as transparent white ribbons, and the selected cofactors are shown as bonds colored green (Chl-*a*), black (Phe-*a*) or cyan (Pl-9). (B and C) Close view of molecules of Chl-*a* (panel B), Phe-*a* (panel C) and Pl-9 (panel D). Carbon atoms are colored cyan, nitrogen – blue and oxygen – red. For clarity, only part of the Pl-9 isoprenyl sidechain is shown explicitly. (For interpretation of the references to color in this figure legend, the reader is referred to the web version of this article.)

The bonded terms include the harmonic terms for the covalent bond stretching and valence angle bending, and terms for dihedral and improper dihedral angles. The harmonic Urey–Bradley coupling term can be included for 1–3 interactions. For the protein backbone, a two-dimensional correction term denoted as the CMAP (energy correction map) was added to reproduce with CHAMM dipeptide energy surfaces computed with high-level quantum mechanics [23]. The nonbonded terms include the Coulomb electrostatic contribution and the van der Waals interactions. In Eq. (1), k_b, k_θ, k_φ, k_ω, and k_{U-B} are the force constants for bond stretching, valence angle bending, dihedral angle torsion, improper angles, and the Urey–Bradley term, respectively. The symbols b, θ, φ, ω, and r_{1-3} indicate the bond lengths, valence angles, dihedral angles and improper angles, and the 1–3 Urey–Bradley distances, with b_0, θ_0, φ_0, ω_0, and $r_{1-3,0}$ the corresponding equilibrium properties. The non-bonded interactions between two atoms i and j separated by the distance r_{ij} are given by the sum of the Coulomb interactions between the atomic partial point charges q_i and q_j, and the van der Waals energy computed as a Lennard–Jones potential, with ε_{ij} the Lennard–Jones well depth and $R_{ij,\min}$ the corresponding distance at the Lennard–Jones minimum. In calculations with explicit solvent, ε is set to 1 (the permittivity of vacuum) [21]. Interactions between atoms separated by one or two covalent bonds (1–2 and 1–3 interactions, respectively) are given by the bond and valence angle terms [21]. Non-bonded interactions between atoms separated by three bonds are not scaled in all-atom CHARMM (i.e., no 1–4 scaling) [21,22].

The force constants, equilibrium values, atomic partial charges, and van der Waals parameters, are part of the force-field parameters. The force-field parameters for a given molecule are derived using data from experiments and/or quantum mechanics (QM) computations on model compounds.

Foloppe et al. [10,11] developed CHARMM force-field parameters for analogs of bacteriochlorophyll and bacteriopheophytin.

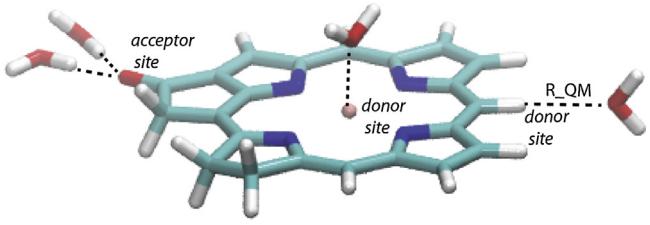

Fig. 2. Illustration of interaction geometries from HF/6-31G* computations of water interaction energies of the Chl-*a* core. The geometry of the Chl-*a* core is optimized with MP2/6-31G*, and the water molecule has TIP3P geometry [16]. The location of the each water molecule relative to the Chl-*a* core corresponds to the lowest-energy value for ΔE_QM. Computations were performed separately for each interaction site. The dotted lines indicate the directions along which the water molecule is constrained during the energy optimization. For the oxygen acceptor site we show the linear interaction pose, and a lone pair interaction. R_QM is the interaction distance.

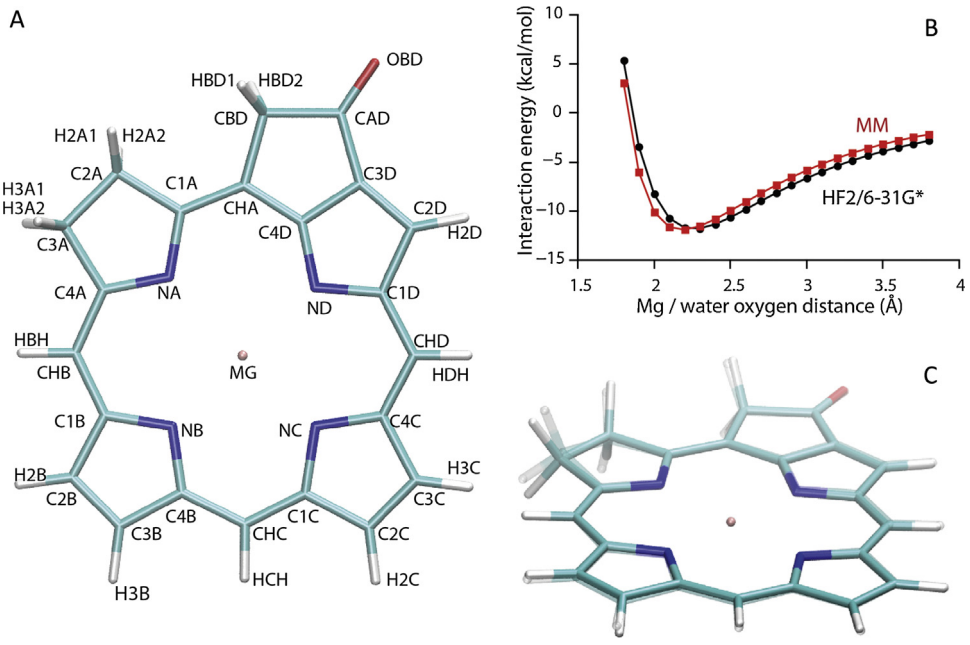

Fig. 3. Geometry and potential energy profile of the Chl-*a* core. (A) Molecular graphics of the MP2-optimized Chl-*a* core with atoms labeled according to the CHARMM atom names. Carbon atoms are colored cyan, oxygen – red, and hydrogen – white. (B) Potential energy profile for the interaction between the magnesium ion and a water molecule. The HF/6-31G* and MM profiles are shown black dots and, respectively, red squares. (C) Overlap of the Chl-*a* core structure optimized with MP2/6-31G* (transparent) vs. MM (full colors). For the MM optimization of the Chl-*a* core, we controlled the planarity of the bond involving atoms H2B, H2C, H3B, H3C, and H2D by using improper angles. These definitions of the improper angles are not needed for the full Chl-*a* molecule, where the H atoms are replaced by sidechains.

Partial atomic charges were derived via Mülliken population analyses using the semi-empirical Hamiltonians AM1 (Austin Model 1, [9]) or PM3 (Parametrized Model number 3, [29]) for bacteriopheophytin [10]) and bacteriochlorophyll, respectively [11]). Parameters for bonded interactions were derived from high-resolution crystal structures data, and by analogy with the CHARMM parametrization of heme-histidine interactions [10,11]. Another set of partial atomic charges for bacteriochlorophyll-*b* and bacteriophytin-*b* models was derived using PM3 and a CHELPG-type (Charges from ELectrostatic Potential using Grid-based method) population analysis [27]. In more recent work, partial atomic charges of bacteriochlorophyll atoms were assigned based on electrostatic potential (ESP) computations with a 6-31G** basis set [8], and using Density Functional Theory (DFT) calculations in Ref. [15a]. The atomic partial charges reported in Refs. [8,15a,27] for the magnesium ion and for the nitrogen atoms of bacteriorchlorophylls are rather different. The magnesium ion has a charge of 0.10*e* in the PM3 computations on bacteriochlorophyll-*b* [27], as compared to 1.03*e* in the ESP computation on bacteriochlorophyll-*a* from Ref. [8], and 0.922 in Ref. [15a]; for the nitrogen atoms, the DFT charges are −0.535 to −0.367 [15a], as compared to values ranging from −0.73*e* to −0.28*e* in Ref. [8].

Good description of the partial atomic charges is required for reliable molecular dynamics simulations of the protein/cofactor complex. Here, we attempt to improve the description of the non-bonded interactions of Chl-*a*, Ph-*a* and Pl-9 by considering the CHARMM philosophy for optimizing atomic partial charges.

The partial atomic charges used in CHARMM are typically optimized such that the water interaction energies computed with CHARMM reproduce values computed with Hartree Fock (HF) with

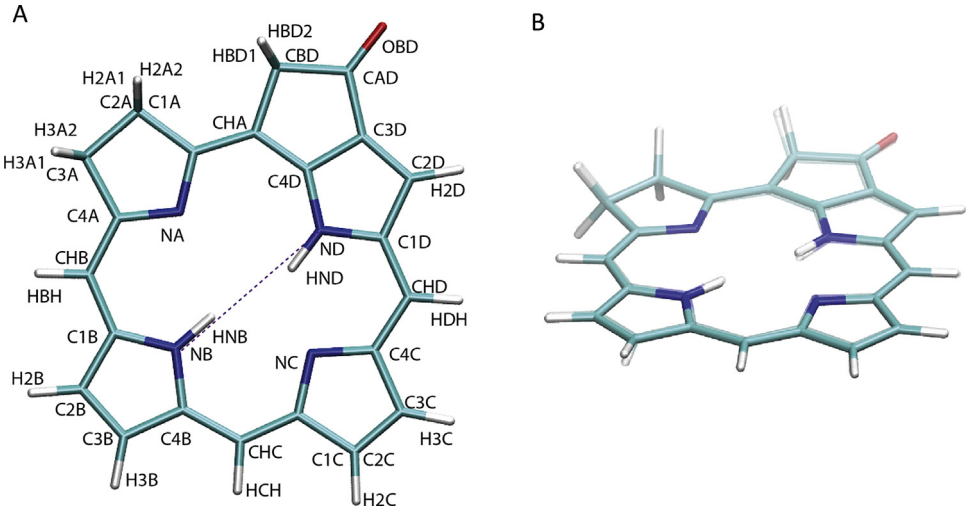

Fig. 4. Geometry and atom names of the Phe-*a* core. (A) Molecular graphics of the MP2-optimized geometry of the Phe-*a* core indicating the atom types. The dotted line illustrates the observation that the NB-HNB and ND-HND are not collinear. (B) Overlap between of the structure of the Phe-*a* core optimized with MP2/6-31G* (transparent) vs. MM (full colors).

a 6-31G* basis set [21]. As described in, e.g., Refs. [21,32], the water interaction energy is computed as the difference between the energy of the water/target molecule complex, and the sum of the energies of the isolated target compound and the water molecule:

$$\Delta E = E_{compound+water} - (E_{compound} + E_{water}) \quad (2)$$

The advantage of optimizing the partial atomic charges based on HF water interaction energies is that the optimized partial charges account implicitly for electronic polarization effects [21].

The CHARMM force field parameters for biomolecules were derived with the TIP3P water model [16,21]. In the CHARMM general force field (CGenFF) [32], the geometry of the isolated target molecule is first optimized with quantum mechanics (QM), e.g., with second-order Moller–Plesset perturbation (MP2) and a 6-31G* basis set. The MP2-optimized geometry of the target molecule is then kept fixed during computations of the water interaction energies, and the geometry of the water molecule is kept fixed to TIP3P; the complexes are geometry-optimized with respect to the distance between the water and the target molecule, separately for each interaction site – that is, for each hydrogen-bond donor and acceptor atom (see example in Fig. 2) [32]. To describe bulk properties and for compatibility with CHARMM, in the case of neutral polar compounds one scales the HF water interaction energies by 1.16, and may offset the HF interaction distance by 0.2 Å [32]. The partial atomic charges in the molecular mechanics (MM) optimization are adjusted iteratively until good agreement is reached between the HF/6-31G* and MM interaction energies for all interaction sites. A standard criterion for the convergence of the MM partial charges is an agreement within 0.2 kcal/mol between water interaction energies computed with HF/6-31G* and MM [32].

We optimized the partial atomic charges for Chl-*a*, Phe-*a* and Pl-9 by performing extensive computations of the water interaction energies. To improve the MM description of the structures of these cofactors, we also adjusted several bonded parameters. The revised parameters we present here describe well the structure and water interactions of the isolated cofactors.

2. Methods

Structural models of the cofactors. Initial coordinates of the cofactors were taken from the crystal structure of photosystem II [31], PDB ID: 3ARC, chain A. For Chl-*a*, Phe-*a* and Pl-9, we used the coordinates for the molecules with the PDB residue numbers 604, 609 and 709, respectively. For computational efficiency, we used core structures in which we replaced all side chains by hydrogen atoms (Figs. 3A, 4A and 5A). Similar considerations have been used before in computations on the heme prosthetic group of cytochrome *c* [2]. Initial coordinates for hydrogen atoms were constructed with the open source tool Avogadro version 1.0.3 [14].

QM geometry optimizations of the core structures of Chl-a, Phe-a and Pl-9. We used MP2/6-31G* to optimize each core structure with the tight tolerance criterion. All QM calculations were performed using Gaussian 09 [12].

MM geometry optimizations. For each molecule, we used the MP2-optimized geometry as starting coordinate set for the CHARMM optimization. MM geometry optimizations were performed to a root-mean squared energy gradient of 10^{-5} kcal/mol Å. We used an infinite cutoff and set ε to 1.0 (see Eq. (1)).

HF/6-31G water interaction energies (ΔE_QM) and distances (R_QM)*. In what follows we use the Chl-*a* core as example to detail the protocol for computing ΔE_QM and R_QM. The same protocol was used for the Phe-*a* and Pl-9 cores.

We used the Force Field Toolkit of VMD [15] to generate Gaussian input files for HF/6-31G* computations of the interaction energies between the MP2-optimized Chl-*a* core and water in TIP3P geometry. The HF/6-31G* geometry optimizations of the Chl-*a* core/water complexes were performed independently for each hydrogen-bond donor (hydrogen and magnesium) and acceptor atoms (oxygen and nitrogen) (see Table 1 and examples in Fig. 2). For the oxygen atom acceptor site of the Chl-*a* and Phe-*a* cores we calculated water interaction energies for the linear geometry, and for an interaction pose whereby the water OH bond interacts with a lone electron pair of the acceptor oxygen atom (Fig. 2).

The lowest-energy value of the interaction energy from the HF/6-31G* computations, scaled by 1.16 [32], is the target QM interaction energy, ΔE_QM. The optimized interaction distance is labeled R_QM (Fig. 2).

MM water interaction energies (ΔE_MM), interaction distances (R_MM), and partial charge optimization. We optimized the MM partial charges by fitting ΔE_MM to ΔE_QM. In what follows we

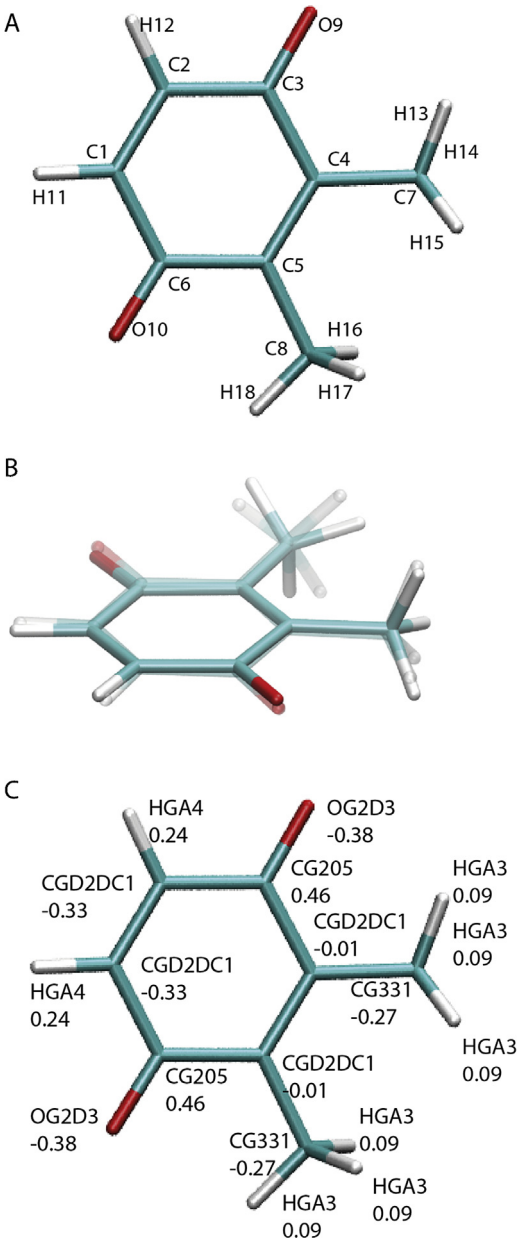

Fig. 5. Geometry and atom names of the Pl-9 core. (A) Molecular graphics of the MP-2 optimized structure of the Pl-9 core with atom names. (B) Overlap of the Pl-9 core structures optimized with MP2/6-31G* (transparent) vs. MM (full colors). (C) Partial atomic charges of the Pl-9 core used for the ΔE_MM calculations reported in Table 8. Atoms are labeled according to the chemical type.

Table 1
Atoms selected for computations of water interaction energies.

Molecule	Atoms used as interaction sites	
Chl-*a* core	NA, NB, NC, ND, OBD, H2A1, H2A2, H2B, H2C, H2D, H3A1, H3A2, H3B, H3C, HBD1, HBD2, HBH, HCH, HDH, MG	Fig. 3A
Phe-*a* core	NA, NB, NC, ND, OBD, H2A1, H2A2, H2B, H2C, H2D, H3A1, H3A2, H3B, H3C, HBD1, HBD2, HBH, HCH, HDH	Fig. 4A
Pl-9	O9, O10, H11, H12, H13, H15, H16, H18	Fig. 5A

describe the protocol used for the Chl-*a* core. The same protocol was used to optimize the partial charges of the Phe-*a* and Pl-9 cores.

To derive the first guess of the MM partial charges we performed a Merz–Kollmann population analysis using the MP2-optimized geometry. To compute the CHARMM water interaction energies between the Chl-*a* core and water we made use of tools from the Force Field Development webpage of the MacKerell Lab, and of the CGenFF protocol from Ref. [32]. For each interaction site, we thus performed an energy optimization of the complex by using as a degree of freedom the distance between the water oxygen atom and the Chl-*a* core; we varied this distance in steps of 0.01 Å, from 1.6 Å to 4.5 Å. The minimum energy value is the MM interaction energy, ΔE_MM, and the corresponding interaction distance is R_MM.

In the next step, we compared ΔE_MM and ΔE_QM. If ΔE_MM and ΔE_QM differed by more than 0.2 kcal/mol, we adjusted manually the partial charges and recalculated ΔE_MM. In adjusting the partial charges we considered local symmetry and the total charge of the molecule, and imposed for the partial charges of the methyl hydrogen and carbon atoms the standard CHARMM values.

Refinement of selected bonded parameters. In CGenFF, the accepted criteria for the deviations between the QM and MM values for bond lengths and valence angles are 0.03 Å and 3°, respectively [32]. In our MM computations on the Chl-*a* core we used for starting bonded parameters values from Refs. [10,11] and from CHARMM. To improve the agreement between the Chl-*a* core geometries optimized with MP2 vs. MM, we adjusted several reference bond lengths and reference valence angles as reported in Section 3.

The Phe-*a* core contains two more hydrogen atoms relative to the Chl-*a* core: HNB and HND (Fig. 4A). For the Phe-*a* core we thus used the same bonded parameters as for the Chl-*a* core, to which we added bonded parameters for HNB and HND as described in Section 3. In the case of the Pl-9 core, all bonded parameters needed for the MM computations were taken from CGenFF and used without further changes. We used CHARMM Lennard–Jones parameters chosen by the similarity of the atom chemical type.

3. Results

3.1. Geometry and water interaction energies of the Chl-a core

The MP2-optimized geometry of the Chl-*a* core, with atoms labeled according to the CHARMM atom names, is depicted in Fig. 3A; the CHARMM chemical types are given in Fig. 6. Starting from this MP2-optimized structure, we calculated the HF and CHARMM water interaction energies for 21 different sites as summarized in Table 4. The ΔE_QM values range from −1.73 kcal/mol for HBD2, to −11.82 kcal/mol for the magnesium ion. We adjusted the partial charges of all atoms of the Chl-*a* core to obtain a good description of ΔE_MM. Similar to the CHARMM description of heme and to the set of bacteriopheophytin partial charges from Ref. [10], we kept the partial charges on atoms CHB, CHC, CHD, HBH, HCH and HDH to −0.10*e* for the carbon atoms, and 0.10*e* for hydrogen atoms (Fig. 6A). Our optimized partial charge of the magnesium ion, 1.17*e* (Fig. 6A), is very close to the average value of 1.18 ± 0.1e derived by Moin and Hofer based on HF/MM simulations of a magnesium-porphyrin compound in water [25].

The mean absolute difference between ΔE_QM and ΔE_MM computed for the 21 interaction sites of the Chl-*a* core (Table 4) is 0.28 kcal/mol. The maximum difference between ΔE_QM and

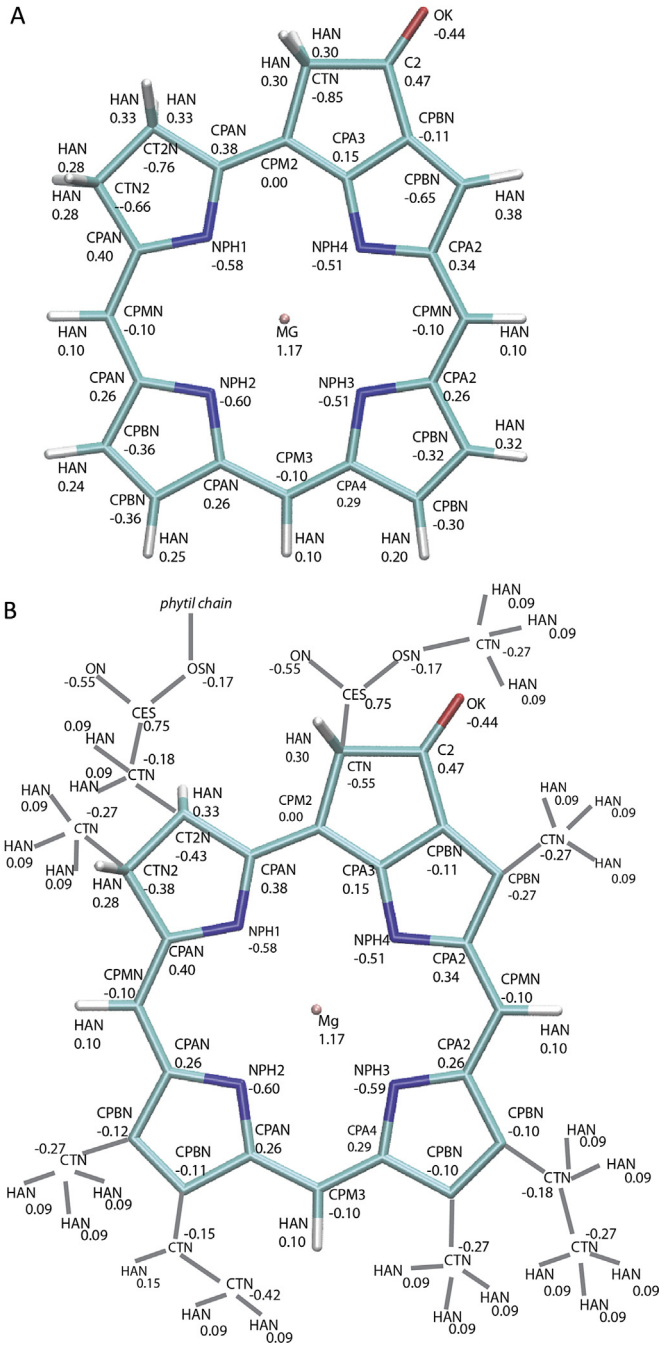

Fig. 6. Atomic partial charges optimized for Chl-*a*. (A) The Chl-*a* core with atom chemical types and atomic partial charges used for computing the ΔE_MM values reported in Table 4. (B) Schematic representation of the complete Chl-*a* molecule. The partial atomic charges of the sidechains were set using the standard CHARMM values for similar compounds. The partial charges of the carbon and hydrogen atoms of the methyl groups are assigned standard CHARMM values.

Table 2
Reference bond lengths (Å) and valence angles (Å) refined for the Chl-*a* core.

Bond/angle	Ref. value, b_0	MP2 value[a]	MM value[a]
Bonds			
CPBN-CPAN	1.437	1.430	1.426
CPBN-CPA2	1.462	1.462	1.455
CPBN-CPA3	1.422	1.420	1.404
CPBN-CPA4	1.467	1.468	1.456
CPBN-CPBN	1.365	1.371	1.363
CPM3-CPAN	1.424	1.439	1.410
CPMN-CPA2	1.400	1.405	1.393
CPM2-CPAN	1.404	1.405	1.417
CPM3-CPA4	1.371	1.371	1.357
NPH4-CPA3	1.385	1.364	1.367
NPH3-CPA4	1.390	1.390	1.375
NPH4-CPA2	1.360	1.365	1.346
NPH1-MG	2.184	2.183	2.167
NPH2-MG	2.028	2.028	2.010
C2-CPBN	1.474	1.481	1.482
Valence angles			
CPA2-CPMN-CPA2	124.827	124.8	127.723
CPAN-NPH2-CPAN	107.35	107.3	108.541
MG-NPH4-CPA2	132.662	132.7	130.650
NPH1-CPAN-CT2 N	110.348	111.4	111.902
NPH2-CPAN-CPMN	124.578	124.6	126.087

The atom chemical types used here are illustrated in Fig. 6A.
[a] Some MM and MP2 bond lengths were averaged as summarized in Table 3.

Table 3
Bonds and valence angles described by the reference bond stretching and angle bending parameters summarized in Table 2.

Bond/angle, atom chemical type[a]	Bonds/angles averaged, atom name[b]
CPBN-CPAN	C1B-C2B; C3B-C4B
CPBN-CPA2	C3C-C4C; C1D-C2D
CPBN-CPA3	C3D-C4D
CPBN-CPBN	C2B-C3B; C2C-C3C; C2D-C3D
CPM3-CPAN	C4B-CHC
CPMN-CPA2	CHD-C1D; CHD-C4C
CPM2-CPAN	CHA-C1A
CMP3-CPA4	CHC-C1C
NPH4-CPA3	ND-C4D
NPH3-CPA4	NC-C1C
NPH4-CPA2	ND-C1D
CPBN-CPA4	C2C-C1C
NPH1-MG	NA-MG
NPH2-MG	NB-MG
C2-CPBN	CAD-C3D
CPA2-CPMN-CPA2	C1D-CHD-C4C
CPAN-NPH2-CPAN	C1B-NB-C4B
MG-NPH4-CPA2	MG-ND-C1D
NPH1-CPAN-CT2N	NA-C1A-C2A, NA-C4A-C3A
NPH2-CPAN-CPMN	NB-C1B-CHB

[a] See labels in Fig. 6A.
[b] See labels in Fig. 3A.

ΔE_MM, 0.51 kcal/mol, is observed for the HCH donor site (Table 4 and Fig. 3A). In the case of the magnesium ion and the carbonyl oxygen atom OBD, ΔE_QM and ΔE_MM agree to within 0.1 kcal/mol and 0.3–0.4 kcal/mol, respectively (Fig. 3A and Table 4).

Overall, there is good agreement between the R_QM and R_MM (Table 4). R_MM for the magnesium ion, 2.18 Å, is close to the R_QM value of 2.26 Å, and to the average value from the crystal structure [31]: the crystal structure (PDB ID: 3ARC, chain A) indicates seven Chl-*a*/water interactions, with an average magnesium/water oxygen distance of 2.1 ± 0.02 Å. In the crystal structure of ethyl chlorophyllide *a* dehydrate, the distance between the magnesium ion and the coordinating water molecule is 2.035 Å [7].

Following optimization of the atomic partial charges, we first tested the MM geometry of the Chl-*a* core by performing a CHARMM geometry optimization without any constraints, using the optimized partial charges reported in Fig. 6A and bonded parameters based on the bacteriopheophytin-*a* parameters from Ref. [11]. To improve the agreement between the structures optimized with MP2 and CHARMM, we then introduced two new chemical atom types, CPA3 and CPA4 (Fig. 6A) and adjusted several bonded parameters as summarized in Tables 2 and 3. The bonded parameters involving the newly introduced atom chemical types CPA3 and CPA4 are the same as for CPAN (Fig. 6A), except for the reference bond lengths whose values, reported in Table 2, were adjusted manually to achieve good agreement between the geometries of the Chl-*a* core optimized with MP2 vs. CHARMM. For atoms C1D and C4C we used the same chemical type, CPA2 (Fig. 6A).

In the next step, we used our optimized partial atomic charges and the bonded parameters with the adjustments described above to perform a MM optimization without constraints. This MM optimization resulted in a structure of the Chl-*a* core that is very close to that optimized with MP2 (Fig. 3C): both the MM- and

Table 4
Water interaction energies (kcal/mol) and interaction distances (Å) computed for the Chl-*a* core.

Interaction site[a]	ΔE_QM[b]	ΔE_MM[c]	ΔE_MM–ΔE_QM	R_QM[b]	R_MM[c]	R_MM–R_QM
NA	−2.44	−2.47	−0.03	2.44	2.09	−0.35
NB	−3.64	−3.83	−0.19	2.37	2.03	−0.34
NC	−3.54	−4.03	−0.49	2.39	2.04	−0.35
ND	−3.35	−3.76	−0.41	2.40	2.09	−0.31
OBD	−5.90	−6.17	−0.27	2.06	1.8	−0.26
OBDp	−5.48	−5.09	0.39	2.06	1.82	−0.24
H2A1	−3.10	−3.19	−0.09	2.53	2.51	−0.02
H2A2	−2.64	−2.90	−0.26	2.53	2.51	−0.02
H2B	−2.34	−2.50	−0.16	2.50	2.52	0.02
H2C	−2.38	−2.07	0.31	2.49	2.55	0.06
H2D	−2.47	−2.22	0.25	2.40	2.45	0.05
H3A1	−2.36	−2.64	−0.28	2.57	2.54	−0.03
H3A2	−2.44	−2.87	−0.43	2.57	2.54	−0.03
H3B	−2.61	−2.54	0.07	2.46	2.51	0.05
H3C	−2.50	−2.26	0.24	2.48	2.53	0.05
HBD1	−1.82	−1.33	0.49	2.56	2.55	−0.01
HBD2	−1.73	−1.32	0.42	2.59	2.57	−0.02
HBH	−2.49	−2.91	−0.41	2.55	2.56	0.01
HCH	−2.95	−2.44	0.51	2.45	2.57	0.12
HDH	−3.15	−3.10	0.05	2.42	2.78	0.36
MG	−11.82	−11.92	−0.10	2.26	2.18	−0.08

[a] The interaction sites are depicted in Fig. 2. OPDp is a lone-pair interaction of OBD.
[b] HF/6-31G* values. ΔE_QM values were scaled by 1.16.
[c] Energy and distance values from MM computations.

Table 5
Comparison between Chl-*a* core structures optimized with MP2 vs. MM.

	MP2	MM
Distances (Å)		
MG-NA	2.18	2.17
MG-NB	2.03	2.01
MG-NC	2.06	2.06
MG-ND	2.03	2.04
Angles (°)		
NA-MG-NC	177.0	178.2
NB-MG-ND	178.2	179.2

For the atom names, see Fig. 3A. The overlap between structures optimized with MP2 vs. CHARMM is given in Fig. 3C.

Table 6
Comparison of selected partial atomic charges of Chl-*a* and bacteriochlorophyll.

Atom type	Partial atomic charge		
	Current set[a]	Set A[b]	Set B[c]
MG	1.17	1.03	0.922
NA	−0.58	−0.33	−0.424
NB	−0.6	−0.73	0.12–0.535
NC	−0.59	−0.28	0.01–0.367
ND	−0.51	−0.51	0.01–0.473

[a] Values from the refined force-field parameters reported here for Chl-*a*. The full set of atomic partial charges is reported in Fig. 6.
[b] Data reported in Ref. [8] for bacteriochlorophyll-*a*.
[c] Data reported in Ref. [15a] for bacteriochlorophyll-*a*.

MP2-optimized geometries of the Chl-*a* core indicate an essentially planar chlorin ring, and the distances between the magnesium ion and the four nitrogen atoms are largely the same in the two structures (Table 5). The deviation between the bond lengths and valence angles in the MM-optimized geometry and the corresponding QM values is 0.01 Å for the bond lengths, and 1.12° for the valence angles.

The dipole moments computed with MM vs. HF have the same direction, with a deviation of 4°. The MM dipole moment does, however, overestimate the HF value by 78.2%. Given the complexity of the Chl-*a* molecule and the large number of interaction sites we consider that, at least in a first approximation, the overall good description of the water interaction energies (Table 4) and of the direction of the dipole moment is satisfactory.

To further probe the usefulness of the parameters proposed here, we performed a potential energy scan for the interaction between the magnesium ion and a water molecule. In the both MM and HF/6-31G* potential energy scans, we kept the Chl-*a* core fixed to its MP2-optimized geometry, and moved the water molecule as a rigid body along a direction perpendicular to the chlorin plane. As illustrated in Fig. 3B, we found good agreement between the HF and MM energy potential profiles. In contrast, coarse estimations using partial charges reported for bacteriochlorophyll models in Refs. [8,15a] (Table 6) indicated water interaction energies of the magnesium ion being underestimated by ~3 kcal/mol.

We used the partial atomic charges optimized for the Chl-*a* core to prepare a CHARMM topology file for the complete Chl-*a* molecule. This involved replacing specific hydrogen atoms with larger chemical groups, and adjusting the charges accordingly. For example, in the Chl-*a* core (Fig. 3A) atom CBD has a charge of −0.85, and HBD1 and HBD2 have charges of −0.30 each. In the complete Chl-*a* molecule, CBD has a charge of −0.55, and HBD2 is replaced by CES (Fig. 6).

The partial charges of the complete Chl-*a* molecule (Fig. 6) could be used for simulations of protein complexes that contain Chl-*a*, such as photosystem II. Our preliminary test computations on the Chl-*a* core coordinated by an imidazole molecule suggest that, in simulations of protein/Chl-*a* complexes, additional bonded constraints may be needed to control the geometry of the chlorin ring and the location of the magnesium ion. Though the conformational dynamics of Chl-*a* in protein environments are unclear, it is plausible that Chl-*a* molecules may sample conformations in which the chlorin ring deviates from planarity. For example, in the crystal structure of ethyl chlorophyllide *a* dihydrate, in which the magnesium ion interacts with a water molecule, the magnesium ion is located 0.39 Å out of the the plane of the chlorin ring [7]. Likewise, observations on porphyrin compounds suggest that, depending on the metal ion, the porphyrin ring can deviate significantly from planarity [24]. Systematic computations on simplified complexes that mimic interactions of Chl-*a* with protein groups, such as histidine or asparagine amino acid residues, would be needed to probe the conformational energy landscape of Chl-*a* and further adjust its force-field parameters for specific protein interactions.

Table 7
Water interaction energies (kcal/mol) and interaction distances (Å) computed for the Phe-*a* core.

Interaction site[a]	ΔE_QM[b]	ΔE_MM[c]	ΔE_MM−ΔE_QM	R_QM[b]	R_MM[c]	R_MM−R_QM
NA	−3.00	−3.40	−0.40	2.44	2.17	−0.27
NB	−2.05	−2.12	−0.07	2.37	2.18	−0.19
NC	−3.34	−3.31	0.03	2.39	2.05	−0.34
ND	−1.88	−2.37	−0.49	2.40	2.29	−0.11
OBD	−5.54	−5.35	0.19	2.06	1.83	−0.23
OBDm	−4.37	−4.45	−0.08	2.00	1.85	−0.15
H2A1	−2.72	−2.39	0.33	2.53	2.54	0.01
H2A2	−2.72	−2.46	0.26	2.53	2.54	0.01
H2B	−2.61	−2.65	−0.04	2.50	2.52	0.02
H2C	−2.22	−1.85	0.37	2.49	2.56	0.07
H2D	−2.66	−2.27	0.39	2.40	2.34	−0.06
H3A1	−2.14	−2.27	−0.13	2.57	2.58	0.01
H3A2	−2.14	−2.29	−0.15	2.57	2.57	0.00
H3B	−2.89	−2.53	0.36	2.46	2.52	0.06
H3C	−2.30	−2.03	0.27	2.48	2.54	0.06
HBD1	−1.88	−1.34	0.54	2.56	2.55	−0.01
HBD2	−1.88	−1.35	0.53	2.59	2.55	−0.04
HBH	−2.54	−3.02	−0.48	2.55	2.54	−0.01
HCH	−3.10	−2.47	0.63	2.45	2.56	0.11
HDH	−3.16	−3.24	−0.08	2.42	2.70	0.28

[a] The interaction sites are illustrated in Fig. 4A. OBDm is a lone pair of atom OBD.
[b] HF/6-31G* values. ΔE_QM is scaled by 1.16.
[c] Interaction energies and distances from MM computations.

Table 8
Comparison between Phe-*a* core structures optimized with MP2 vs. MM.

	MP2	MM
Distances (Å)		
NA-NC	4.22	4.35
NB-ND	4.08	4.23
Valence angles (°)		
NB-HNB-ND	177.4	178.7
NB-HND-ND	161.7	170.0
C1B-NB-HND	125.1	126.9
C4B-NB-HNB	124.2	121.8
C1D-ND-HND	120.1	121.8
C4D-ND-HND	130.5	127.1
Improper angles (°)		
C1D-HND-C4D-ND[a]	0.0	0.0
C1B-C4B-HNB-NB[a]	0.0	0.1

The atoms are labeled in Fig. 4A, and the overlap between structures optimized with MP2 vs. CHARMM is given in Fig. 4B.

[a] Improper angles used to measure pyramidality of the NB and ND atoms [4].

3.2. Geometry and water interaction energies of the Phe-a core

The MP2-optimized geometry of the Phe-*a* core is depicted in Fig. 4A with the atoms types used; the CHARMM chemical types are given in Fig. 7. The water interaction energy computations are summarized in Table 7.

We adjusted iteratively the partial charges for the atoms of the Phe-*a* core until we obtained an overall good agreement between ΔE_QM and ΔE_MM, and between R_QM and R_MM (Table 7). The mean absolute difference between ΔE_QM and ΔE_MM computed for all interactions sites of the Phe-*a* core is 0.29 kcal/mol. For the OBD acceptor site, ΔE_MM and ΔE_QM agreed to within 0.2 kcal/mol. For the HCH, HBD1 and HBD2 interaction sites the difference between ΔE_QM and ΔE_MM (0.53–0.63 kcal/mol) is somewhat worse, though still close to ~1 kT (Table 7).

The NB-HNB and ND-HND bonds of the MP2 structure are co-planar with the chlorin ring, but the two bonds are not co-linear (Fig. 4A and Table 8). The NB-HNB bond is almost along the bisector of the C1B-NB-C4B valence angle, with C1B-NB-HNB and C4B-NB-HNB angles of 124–125°. In contrast, the ND-HND bond orients slightly toward NC, such that the C1D-ND-HND and C4-ND-HND valence angles are 120.1° and 130.5°, respectively (Table 8). To reproduce with MM these features of the MP2-optimized structure, during the MM geometry optimizations we adjusted the reference valence bond angles (θ_0) for HND-ND-C4D to 120.5°, and that for HND-ND-C1D to 130.5°. θ_0 for the C1B-NB-HNB and C4B-NB-HNB valence bond angles was kept to the CGenFF value of 125.5°. All other bonded parameters involving HNB and HND (Fig. 4A) were taken from CGenFF. Comparison of the Phe-*a* structures optimized with MP2 vs. MM indicates agreement within 3° for the valence angles involving HNB and HND (Table 8).

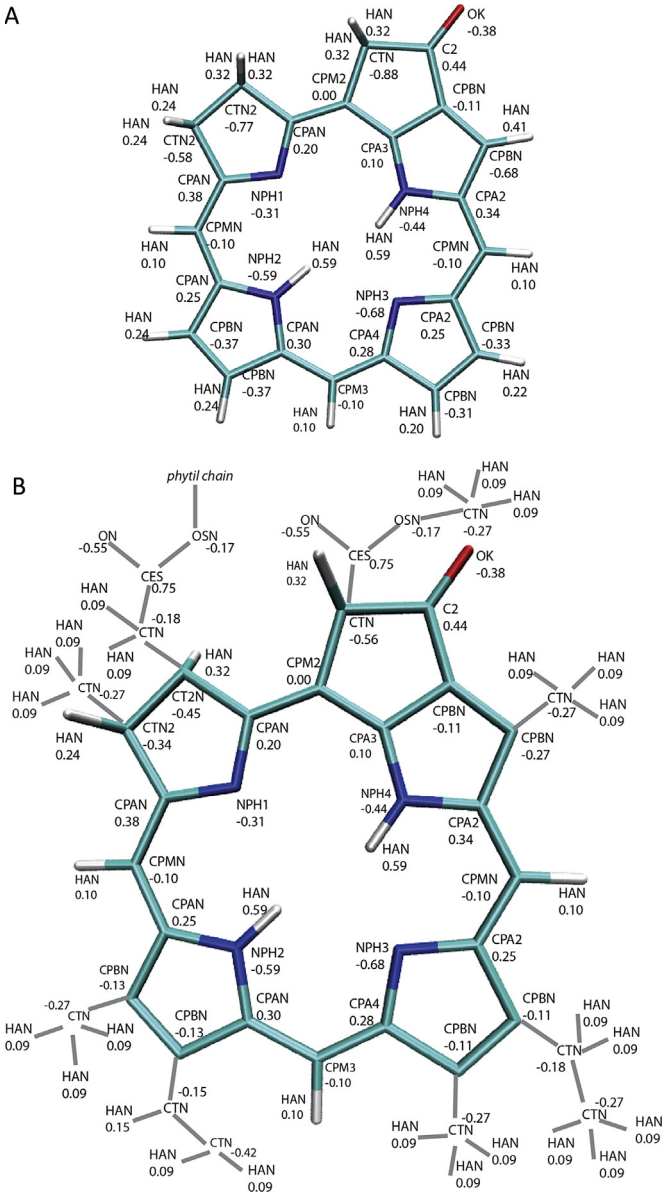

Fig. 7. Partial atomic charges optimized for Phe-*a*. (A) The Phe-*a* core with atom chemical types and atomic partial charges used for computing the ΔE_MM values reported in Table 6. (B) The complete Phe-*a* molecule with partial charges adjusted as described for Chl-*a*, using partial charges from Figure 7A and from the CHARMM force field.

Table 9
Water interaction energies (kcal/mol) and distances (Å) computed for the Pl-9 core.

Interaction site[a]	ΔE_QM[b]	ΔE_MM[c]	ΔE_QM–ΔE_MM	R_QM[b]	R_MM[c]	R_MM–R_QM
O9	−4.14	−4.29	−0.15	2.12	1.75	−0.37
O10	−4.13	−4.28	−0.15	2.12	1.75	−0.37
H11	−2.71	−2.53	0.18	2.37	2.48	0.11
H12	−2.70	−2.53	0.17	2.37	2.48	0.11
H13	−2.31	−1.49	0.82	2.66	2.70	0.04
H15	−1.97	−1.29	0.68	2.59	2.69	0.10
H16	−2.31	−1.49	0.82	2.66	2.70	0.04
H18	−1.97	−1.29	0.68	2.59	2.69	0.10

[a] The interaction sites are depicted in Fig. 5A.

[b] HF/6-31G* values. The ΔE_QM values were scaled by 1.16. Since the atomic partial charges of the carbon and hydrogen atoms of the methyl groups are set to the standard CHARMM values, we did not perform computations for atoms H14 and H17.

[c] Interaction energies and distances from MM calculations.

3.3. Geometries and water interaction energies of the Pl-9 core

The MP2-optimized geometry and the atoms names used for the Pl-9 core are depicted in Fig. 5A, and the CHARMM chemical types are given in Fig. 5C. The results of the water interaction energy computations are summarized in Table 9. We adjusted the partial charges of the Pl-9 core subject to the constraint that the carbon and hydrogen atoms of the two methyl groups have standard CHARMM charges of −0.27 (for carbon) and 0.09 (hydrogen). With these constraints, we could obtain an overall good agreement between ΔE_QM and ΔE_MM (Table 9). There is good agreement, to within 0.2 kcal/mol, between ΔE_QM and ΔE_MM values of the oxygen acceptor sites (O9 and O10), and of the donor sites H11 and H12 (Table 9). Comparison of the geometries of Pl-9 core optimized with MM vs. MP2 indicates good agreement for the coordinates of the ring atoms (Fig. 5B).

4. Conclusions

We revised the CHARMM force field description of the Chl-*a*, Phe-*a* and Pl-9 cofactors. We optimized the partial atomic charges of the three cofactor molecules by fitting the MM water interaction energies to values from HF/6-31G* computations, and adjusted bonded parameters to improve the description of the cofactor structures. Overall, there is good agreement between the CHARMM and HF/6-31G* water interaction energies. In the case of the Chl-*a* core, we gave particular attention to describing the water interaction energies of the magnesium ion and of the oxygen acceptor sites, where in the protein environment there can be interactions with water or other protein groups. Potential energy scans performed with HF/6-31G* and MM for the interaction between the magnesium ion and a water molecule indicate good agreement (Fig. 3B). Pursuant to these considerations, we suggest that the revised parameters presented here will allow a better description of the structures and nonbonded interactions between the cofactor molecules and protein groups in protein/cofactor complexes such as photosystem II.

Acknowledgements

Computations using Gaussian 09 were performed using a computing time allocation from the North-German Supercomputing Alliance (HLRN bec00063, to A-NB) and on the Soroban cluster of the Freie Universität Berlin. We acknowledge Mr. Florian Pieront and Mr. Abdal-Azim Al-Terkawi for some preliminary tests that were not included here, and Mr. Christopher Mielack for curating the CHARMM topology files. This work was supported in part by the German Research Foundation (DFG) Collaborative Research Center SFB 1078 'Protonation Dynamics in Protein Function' Project C4 (to A-NB). A-NB is supported in part by the Marie Curie International Reintegration Award IRG-276920. We are grateful to Dr. Ana Damjanovic for the starting topology and parameter files of bacteriochlorophyll and bacteriopheophytin based on Refs. [8,10,11]. We thank Prof. Ernst-Walter Knapp for a topology file for photosystem II, and Prof. Jeremy C. Smith for helpful discussions.

References

[1] S.I. Allakverdiev, T. Tomo, Y. Shimada, H. Kindo, R. Nagao, V. Klimov, M. Mimuro, Redox potential of pheophytin a in photosystem II of two cyanobacteria having the different special pair chlorophylls, Proc. Natl. Acad. Sci. U. S. A. 107 (2010) 3924–3929.
[2] F. Autenrieth, E. Tajkhorshid, J. Baudry, Z. Luthey-Schulten, Classical force field parameters for the heme prosthetic group of cytochrome c, J. Comput. Chem. 25 (2004) 1613–1622.
[3] J. Barber, Photosynthetic energy conversion: natural and artificial, Chem. Soc. Rev. 38 (2009) 185–196.
[4] A.-N. Bondar, M. Knapp-Mohammady, S. Suhai, S. Fischer, J.C. Smith, Ground-state properties of the retinal molecule: from quantum mechanical to classical mechanical computations of retinal proteins, Theor. Chem. Acc. 130 (2011) 1169–1183.
[5] B.R. Brooks, R.E. Bruccoleri, B.D. Olafson, D.J. States, S. Swaminathan, M. Karplus, CHARMM: a program for macromolecular energy, minimization, and dynamics, J. Comput. Chem. 4 (1983) 187–217.
[6] B.R. Brooks, C.L.I. Brooks, A.D. MacKerell Jr., L. Nilsson, R.J. Petrella, B. Roux, Y. QWon, G. Archontis, C. Bartels, S. Boresch, A. Caflisch, L. Caves, Q. Cui, A.D. Dinner, M. Feig, S. Fischer, J. Gao, M. Hodoscek, W. Im, K. Kuczera, T. Lazaridis, J. Ma, V. Ovchinnikov, E. Paci, R.W. Pastor, C.B. Post, J.Z. Pu, M. Schaefer, B. Tidor, R.M. Venable, H.L. Woodcock, X. Wu, W. Yang, D.M. York, M. Karplus, CHARMM: the biomolecular simulation program, J. Comput. Chem. 30 (2009) 1545–1614.
[7] H.-C. Chow, R. Serlin, C.E. Strouse, The crystal and molecular structure and absolute configuration of ethyl chlorophyllide a dihydrate. A model for the different spectral forms of chlorophyll a, J. Am. Chem. Soc. 97 (1975) 7230–7237.
[8] A. Damjanovic, I. Kosztin, U. Kleinekathöfer, K. Schulten, Excitons in a photosynthetic light-harvesting system: a combined molecular dynamics, quantum chemistry, and polaron model study, Phys. Rev. E 65 (2002) 031919.
[9] M.J.S. Dewar, E.G. Zoebisch, E.F. Healy, J.J.P. Stewart, AM1: a new general purpose quantum mechanical molecular model, J. Am. Chem. Soc. 107 (1985) 3902–3909.
[10] N. Foloppe, J. Breton, J.C. Smith, Potential energy function for photosynthetic reaction centre chromophores: energy minimisations of a crystalline bacteriophytin A analog, in: J. Brenton, A. Vermeglio (Eds.), The Photosynthetic Bacterial Reaction Center II, Plenum Press, New York, 1992.
[11] N. Foloppe, M. Ferrand, J. Breton, J.C. Smith, Structural model of the photosynthetic reaction center of rhodobacter capsulatus, Proteins: Struct. Funct. Gen. 22 (1995) 226–244.
[12] Frisch, M.J., Trucks, G.W., Schlegel, H.B., Scuseria, G.E., Robb, M.A., Cheeseman, J.R., Scalmani, G., Barone, V., Mennucci, B., Petersson, G.A., KNakatsuji, H., Caricato, M., Li, X., Hratchian, H.P., Izmaylov, A.F., Bloino, J., Zheng, G., Sonnenberg, J.L., Hada, M., Ehara, M., Toyota, K., Fukuda, R., Hasegawa, J., Ishida, M., Nakajima, T., Honda, Y., Kitao, O., Nakai, H., Vreven, T., Montgomery Jr., J.A., Peralta, J.E., POgliaro, F., Beapark, M., Heyd, J.J., Brothers, E., Kudin, K.N., Staroverov, V.N., Kobayashi, R., Normand, J., Raghavachari, K., Rendell, A., Burant, J.C., Iyengar, S.S., Tomasi, J., Cossi, M., Rega, N., Millam, J.M., JKlene, M., Knox, J.E., Cross, J.B., Bakken, V., Adamo, C., Jaramillo, J., Gomperts, R., Stratmann, R.E., Yazyev, O., Austin, A.J., Cammi, R., Pomelli, C., Ochterski, J.W., Martin, R.L., Morokuma, K., Zakrzewski, V.G., Voth, G.A., Salvador, P., Dannenberg, J.J., Dapprich, S., Daniels, A.D., Farkas, O., Foresman, J.B., Ortiz, J.V., Ciosliwski, J., Fox, D.J., 2009. Gaussian, Inc., Wallingford CT.
[13] P. Fromme, P. Jordan, N. Krauß, Structure of photosystem I, Biochim. Biophys. Acta 1507 (2001) 5–31.
[14] M.D. Hanwell, D.E. Curtis, D.C. Lonie, T. Vandermeersch, E. Zurek, G.R. Hutchison, Avogadro: an open-source molecular builder and visualization tool, J. Cheminfo. 4 (2012) 17.
[15] W. Humphrey, W. Dalke, K. Schulten, VMD: visual molecular dynamics, J. Mol. Graph. 14 (1996) 33–38.
[15a] H. Ishikita, B. Loll, J. Biesiadka, A. Galstyan, W. Saenger, E.-W. Knapp, Tuning electron transfer by ester-group of chlorophylls in bacterial photosynthetic center, FEBS Lett. 579 (2005) 712–716.
[16] W.L. Jorgensen, J. Chandrasekhar, J.D. Madura, R.W. Impey, M.L. Klein, Comparison of simple potential functions for simulating liquid water, J. Chem. Phys. 79 (1983) 926–935.
[17] V.V. Klimov, A.V. Klevanik, V.A. Shuvalov, A.A. Krasnovsky, Reduction of pheophytin in the primary light reaction of photosystem II, FEBS Lett. 82 (1977) 183–186.
[18] P. Kühn, J. Pieper, O. Kaminskaya, K.-J. Eckert, V. LechnerShuvalov, G. Renger, Reaction pattern of photosystem II: oxidative cleavage and protein flexibility, Photosynth. Res. 84 (2005) 317–323.
[19] C. Kupitz, S. Basu, I. Grotjohann, R. Fromme, N.A. Zatsepin, K.N.R. JHunter, M.S. Shoeman, R.L. White, T.A. Wang, D. James, D. Yang, J.-H. Cobb, D.E. Reeder, B. Sierra, R.G. Liu, H. Barty, A. Aquila, A.L. Deponte, D. Kirian, R.A. Bari, S. Berkgkamp, J.J. Beyerlein, K.R. Bogan, M.J. Caleman, C. Chao, T.-C. Conrad, C.E. Davis, K.M.H.L. Fleckenstein, G. Hau-Riege, S.P. Kassemeyer, S. Laksmono, H. Liang, M. Lomb, L. Marchesini, S. Martin, A.V. Messerschmidt, M. Milathianaki, D. Nass, K. Ross, A. Roy-Chowdhury, S. Schmidt, K. Seibert, M.M. Steinbrener, J. Stellato, F. Yan, L. Yoon, C. Moore, T.A. Moore, A.L. Pushkar, Y. Williams, G.J. Boutet, S. Doak, R.B. Weiestall, U. Frank, M. Chapman, H.N. Spence, J.C.H.P. Fromme, Serial time-resolved crystallography of photosystem II using a femtosecond X-ray laser, Nature 513 (2014) 261–265.
[20] B. Loll, J. Kern, W. Saenger, A. Zouni, J. Biesiadka, Towards complete cofactor arrangement in the 3.0 Å resolution structure of photosystem II, Nature 438 (2005) 1040–1044.
[21] A.D. MacKerell Jr., Empirical force fields for biological molecules: overviews and issues, J. Comput. Chem. 25 (2004) 1584–1604.
[22] A.D. MacKerell Jr., D. Bashford, M. Bellot, R.L. Dunbrack, J.D. Evanseck, S. Fischer, J. Gao, H. Guo, S. Ha, D. Joseph-McCarthy, L. Kuchnir, K. Kukzera, F.T.K. Lau, C. Mattos, S. Michnick, T. Ngo, D.T. Nguyen, B. Prodhom, W.E.I. Reiher, B. Roux, M. Schlenkrich, J.C. Smith, R. Stote, J. Straub, M. Watanabe, J. Wiorkiewicz-Kukzera, D. Yin, M. Karplus, All-atom empirical potential for molecular modeling and dynamics studies of proteins, J. Phys. Chem. B 102 (1998) 3586–3616.
[23] A.D. MacKerell Jr., M. Feig, C.L.I. Brooks, Extending the treatment of backbone energetics in protein force fields: limitations of gas-phase quantum mechanics

in reproducing protein conformational distributions in molecular dynamics simulations, J. Comput. Chem. 25 (2004) 1400–1415.
[24] H.M. Marques, K.L. Brown, Molecular mechanics and molecular dynamics simulations of porphyrins, metalloporphyrins, heme proteins and cobalt corrinoids, Coord. Chem. Rev. 225 (2002) 123–158.
[25] S.T. Moin, T.S. Hofer, Hydration of porphyrin and Mg-porphyrin: ab ainitio quantum mechanical charge field moecular dynamics simulations, Mol. Biosyst. 10 (2014) 117–127.
[26] W.W. Parson, Photosynthetic bacterial reaction centers: interactions among the bacteriochlorophylls and bacteriopheophytins, Ann. Rev. Biophys. Bioenerg. 11 (1982) 57–80.
[27] B. Rabenstein, G.M. Ullmann, E.-W. Knapp, Calculation of protonation patterns in proteins with structural relaxation and molecular ensembles – application to the photosynthetic reaction center, Eur. Biophys. J. 27 (1998) 626–637.
[28] D. Schulze-Siebert, U. Homeyer, J. Soll, G. Schultz, Synthesis of plastoquinone-9, a-tocopherol and phylloquinone (vitamin K1) and its integration in chloroplast carbon metabolism of higher plants, in: P.K. Stumpf, J.B. Mudd, W.D. Nes (Eds.), The Metabolism, Structure and Function of Plant Lipids, Plenum Press, New York/London, 1986, pp. 29–36.
[29] J.J.P. Stewart, Optimization of parameters for semiempirical methods, J. Comput. Chem. 10 (1989) 209–220.
[30] M. Suga, F. Akita, K. Hirata, G. Ueno, H. Murakami, Y. Nakajima, T. Shimizu, K. Yamashita, M. Yamamoto, H. Ago, J.-R. Shen, Native structure of photosystem II at 1.95 Å resolution viewed by femtosecond X-ray pulses, Nature (2014).
[31] Y. Umena, K. Kawakami, J.-R. Shen, N. LKamiya, Crystal structure of oxygen-evolving photosystem II at a resolution of 1.9 Å, Nature 473 (2011) 55–60.
[32] K. Vanommenslaeghe, E. Hatcher, C. Acharya, S. Kundu, S. Zhong, J. Shim, E. Darian, O. Guvench, P. Lopes, I. Vorobyov, A.D. MacKerell Jr., CHARMM additive general force field: a force field for drug-like molecules compatible with the CHARMM all-atom additive biological force fields, J. Comput. Chem. 31 (2010) 671–690.